Monitoring RNA Base Structure and Dynamics Using Site-Directed Spin Labeling†

Peter Z. Qin,‡,§,|| Kálmán Hideg,⊥ Juli Feigon,§ and Wayne L. Hubbell*,‡,§

Jules Stein Eye Institute and Department of Chemistry and Biochemistry, University of California, Los Angeles, Los Angeles, California 90095, Department of Chemistry, University of Southern California, LJS-251, 840 Downey Way, Los Angeles, California 90089-0744, and Institute of Organic and Medical Chemistry, University of Pécs, P.O. Box 99, H-7643 Pécs, Hungary

Received November 21, 2002; Revised Manuscript Received April 14, 2003

ABSTRACT: Site-directed spin labeling utilizes site-specific attachment of a stable nitroxide radical to probe the structure and dynamics of macromolecules. In the present study, a 4-thiouridine base is introduced at each of six different positions in a 23-nucleotide RNA molecule. The 4-thiouridine derivatives were subsequently modified with one of three methanethiosulfonate nitroxide reagents to introduce a spin label at specific sites. The electron paramagnetic resonance spectra of the labeled RNAs were analyzed in terms of nitroxide motion and the RNA solution structure. At a base-paired site in the RNA helix, where the nitroxide has weak or no local interactions, motion of the nitroxide is apparently dominated by rotation about bonds within the probe. The motion is similar to that found for a structurally related probe on helical sites in proteins, suggesting a similar mode of motion. At other sites that are hydrogen bonded and stacked within the helix, local interactions within the RNA molecule modulate the nitroxide motion in a manner consistent with expectations based on the known structure. For a base that is not structurally constrained, the mobility is higher than at any other site, presumably due to motion of the base itself. These results demonstrate the general utility of the 4-thiouridine/methanethiosulfonate coupling method to introduce nitroxide spin labels into RNA and the ability of the resulting label to probe local structure and dynamics.

RNA is a versatile molecule that plays multiple roles in gene expression and acts as an information carrier, catalyst, and regulator (*1*). Many aspects of RNA function depend on its ability to form compact and complex three-dimensional structures. During the past 5 years, there has been an explosion of high-resolution RNA structures, increasing the size of the database of known RNA structures (*2*). However, to elucidate structure−function relationships, it is necessary to go beyond the static structure and understand the dynamics of the molecule in solution. For this purpose, it is essential to develop spectroscopic tools that provide information on both fluctuations of the structure at equilibrium and conformational changes. Picosecond to nanosecond motions in RNA bases have been studied by NMR spectroscopy (*3*−*5*). Conformational rearrangements of RNA loops in the microsecond to millisecond regime have been studied by both NMR spectroscopy (*6*) and fluorescence spectroscopy (*7*). Conformational changes of large RNA molecules on the millisecond or slower time scales have been probed by fluorescence spectroscopy (*8*−*12*) and chemical modification footprinting (*13*, *14*). These studies reveal an enormous complexity in RNA dynamics and show that there is a general correlation between RNA dynamics, structure, and function.

The technique of SDSL[1] has been developed to study structure and dynamics in proteins (*15*−*21*). The basic strategy of SDSL in proteins involves the substitution of a cysteine for the native residue, followed by modification of the reactive SH group with a selective paramagnetic nitroxide reagent. The most commonly employed reagent is a methanethiosulfonate derivative that generates a disulfide-linked nitroxide side chain. Analyzing the EPR spectrum of the labeled protein yields information on three aspects of interest: (1) the dynamics of the nitroxide (i.e., the overall rotational motion of the nitroxide); (2) the collision rate between the nitroxide and a freely diffusing paramagnetic agent, a quantity proportional to the solvent accessibility; and (3) the distance between the nitroxide and another paramagnetic species fixed in the structure. Methods have

† Research reported here was supported by NIH Grant EYO5216 (W.L.H.), the Jules Stein Professor Endowment (W.L.H.), the Bruce Ford Bundy and Anne Smith Bundy Foundation (W.L.H.), NSF Grant MCB-9808072 (J.F.), NIH Grant R01 GM 37254 (J.F.), the Hungarian National Research Foundation (OTKA T034307 to K.H.), and the startup fund from the University of Southern California (P.Z.Q.). P.Z.Q. was a DuPont Pharmaceutical Fellow of the Life Sciences Research Foundation.

* To whom correspondence should be addressed at the Jules Stein Eye Institute, UCLA School of Medicine, 100 Stein Plaza, Los Angeles, CA 90095-7008. Tel: (310) 206-8830. Fax: (310) 794-2144. E-mail: hubbellw@jsei.ucla.edu.

‡ Jules Stein Eye Institute, University of California, Los Angeles.

§ Department of Chemistry and Biochemistry, University of California, Los Angeles.

|| Department of Chemistry, University of Southern California.

⊥ Institute of Organic and Medical Chemistry, University of Pécs.

[1] Abbreviations: buffer A, 10 mM sodium phosphate, pH 6.8; DTT, DL-dithiothreitol; EPR, electron paramagnetic resonance; MMTS, methylmethanethiosulfonate; MOPS, 3-(*N*-morpholino)propanesulfonic acid; SDSL, site-directed spin labeling; T4L, T4 lysozyme; TEMPOL, 1-oxy-4-hydroxy-2,2,6,6-tetramethylpiperidine; TLC, thin-layer chromatography.

10.1021/bi027222p CCC: $25.00
Published on Web 05/15/2003

been established to extract protein structural and dynamic information from these parameters. For example, the motion of the nitroxide side chain can provide information on backbone dynamics (*21*, *22*) and conformational changes (*19*), while the sequence dependence of solvent accessibility identifies regular secondary structure and features of the tertiary fold (*23*). The interspin distance between two nitroxides, or between a nitroxide and a fixed paramagnetic metal ion, provides direct structural data (*24*−*28*).

SDSL allows one to deduce key structural features of a protein at the backbone level and, more importantly, to follow structural changes by monitoring the time-dependent variation of the spectral parameters of a spin label. The scope and capabilities of the method have been demonstrated in studies of many proteins, especially membrane or membrane-associated proteins that are difficult to tackle with other techniques. With the advantage of being able to gain information from a small amount of sample (~100 pmol) in solution conditions, SDSL should also be an ideal technique for studying RNA structure and dynamics.

SDSL has only recently been applied to study RNA (*29*−*32*). Because SDSL is a method that relies on external reporter groups, efficient attachment of the spin label to RNA is critical. Labeling at RNA backbone locations has been achieved by introducing a site-specific phosphorothioate group and subsequent reaction with an α,β-unsaturated iodomethane derivative of a nitroxide (*31*). Spin labels have also been attached to the 5′ terminus of RNA by taking advantage of a 5′-phosphorothioate (*29*). Substitution of specific 2′-hydroxyl groups with amine groups allows the attachment of nitroxides at specific sugar positions (*30*). Attachment of nitroxides to modified RNA bases using iodoacetamide reagents has also been reported (*33*).

Currently, most SDSL studies of RNA have focused on deriving RNA structural information from the motion of the nitroxide (*30*−*32*). The overall motion of a nitroxide in a macromolecule is determined by three dynamic modes: (1) the rotation of the entire molecule (characterized by correlation time τ_R); (2) torsional oscillations about bonds that connect the nitroxide moiety to the macromolecule; and (3) structural fluctuations within the macromolecule. Although τ_R does not contain site-specific information, changes of τ_R can be used to probe RNA/RNA interactions in solution (*31*). On the other hand, the other motions reflect the RNA local environment and dynamics.

The point of attachment and the structure of the probe dictate the type of information that can be obtained. In RNA, the nucleobase and the sugar ring are connected by a glycosidic bond, and in general, the base and the sugar have different dynamic characteristics. To probe base dynamics, it is therefore important to develop methods to attach nitroxide probes directly to the RNA base. The naturally occurring 4-thiouridine modification, which contains a reactive thiol group and can be incorporated into RNA both enzymatically or via chemical synthesis, provides an attractive target for spin labeling. An iodoacetamide spin label derivative has been employed to attach a spin label to a 4-thiouridine base for the purpose of obtaining distance constraints in NMR studies of an RNA/protein complex (*33*). However, the sensitivity of the spin label to local RNA structure and dynamics has not been investigated.

The goals of the present study are twofold: (1) to devise a method to attach nitroxide spin labels to specific base positions within an RNA molecule and (2) to investigate the correlation between the nitroxide motion and the RNA base structure and dynamics. For attachment of spin labels to RNA, it is shown that thiol-reactive methanethiosulfonate nitroxide reagents, which have been extensively investigated in protein studies (*15*), selectively derivatize a site-specifically substituted 4-thio-U base (Figure 1A). Thus, the spin-labeled 4-thio-U base itself is employed as a probe, and evidence is presented to show that the motion of the nitroxide reflects both local RNA structure and the dynamics of the base to which it is attached.

To explore the utility of the probes as monitors of RNA structure and dynamics, a 23-nucleotide RNA molecule (Figure 1B), which contains the 11-nucleotide GAAA tetraloop receptor motif (*34*) capped by an UUCG terminal loop, was selected as a model. In keeping with previous literature, this RNA is hereafter referred to as "TLR" (*35*). Although there are less complex structures available, TLR was selected because the solution structure has been obtained by NMR (*35*) and the dynamics of the UUCG loop investigated (*3*). The RNA provides several different arrangements of U nucleotides (Watson−Crick paired, non-Watson−Crick paired, unpaired) to test the utility of the spin label in probing different environments. In addition, the GAAA tetraloop receptor motif is a component of one of the most frequently occurring RNA tertiary interactions: the GAAA tetraloop/receptor interaction (*34*). Spin labeling studies reported here provide a foundation for future investigation of the GAAA tetraloop/receptor interaction using the SDSL method.

EPR spectral analyses show that at a base-paired site in the RNA helix, where the nitroxide has weak or no local interactions, the motion of the nitroxide in label Ra (Figure 1A) is constrained and apparently dominated by the rotation about bonds within the nitroxide probe. The motion is essentially identical to that found for a similar label on helical surface sites in proteins, suggesting a similar origin. At other base-paired sites, local interactions within the RNA molecule modulate this motion in a manner consistent with expectations based on the known structure. Finally, at a previously identified non-base-paired site in the UUCG tetraloop, the nitroxide shows the highest mobility observed, presumably reflecting the motion of the base itself.

MATERIALS AND METHODS

RNA Preparation. The sequence of TLR is 5′GGCCUAAGACUUCGGUUAUGGCC. TLR molecules containing singly substituted 4-thiouridine at positions 5, 11, 12, 16, 17, and 19 (numbering from 5′ terminus) are designated 4-thio-U*x*-TLR, where *x* indicates the position of substitution. The 4-thio-U*x*-TLR molecules were obtained from Dharmacon Research, Inc. (Lafayette, CO) and deprotected according to protocols provided by the vendor. For NMR studies, TLR was generated enzymatically as reported (*35*). All RNAs were purified by denaturing polyacrylamide gel electrophoresis.

Synthesis of Spin-Labeling Reagents. General. Melting points were determined on a Boetius micro-melting point apparatus and are uncorrected. Elemental analyses (C, H,

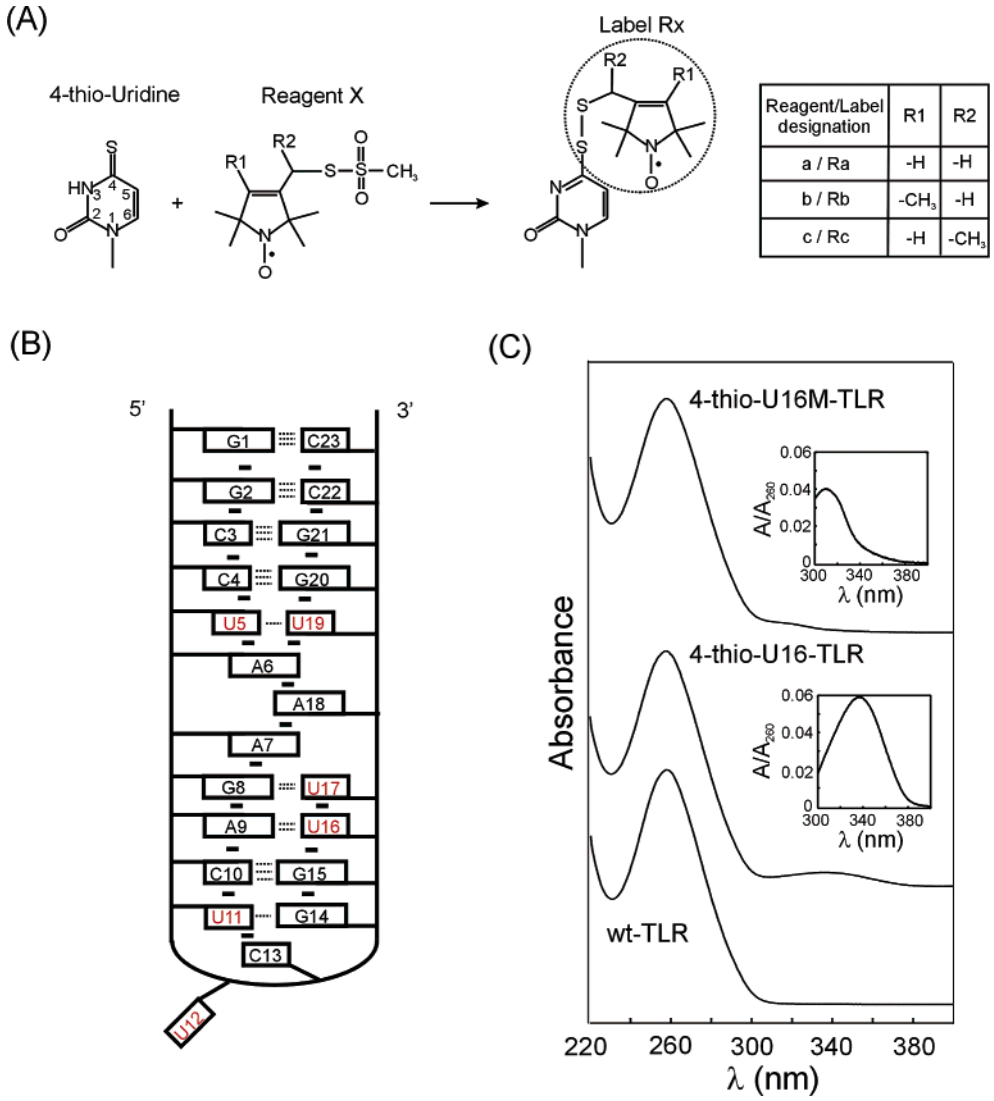

FIGURE 1: (A) 4-Thiouridine labeling scheme. An uridine base is substituted by 4-thiouridine during chemical synthesis and subsequently labeled with methanethiosulfonate derivatives **a**, **b**, or **c** to generate the corresponding labels Ra, Rb, or Rc. (B) Sequence and secondary structure of the TLR molecule. The bases are represented by open rectangles and numbered from 5′ to 3′. Dashed lines between bases represent hydrogen bonds. Small black rectangles between bases represent stacking interactions. The six uridines within the TLR are shown in red. (C) Absorbance spectra of wild-type and modified TLR. Representative spectra between 220 and 400 nm are shown for TLR molecules with modifications at U16, and the difference spectra between wild-type and modified TLR are shown in the corresponding insets.

N, and S) were performed on EA 1110 CHNS elemental analyzer, and the bromine was analyzed tritrimetrically by Schöniger's method. IR spectra were recorded on a Zeiss Specord 75. Mass spectra were recorded on a Finnigan Automass Multi instrument.

The thiol-reactive reagent **a** [1-oxyl-3-(methanesulfonylthiomethyl)-2,5-dihydro-2,2,5,5-tetramethyl-1*H*-pyrrole] was synthesized as reported (*36*), and the thiol-reactive reagent **b** [1-oxyl-3-(methanesulfonylthiomethyl)-2,5-dihydro-2,2,4,5,5-pentamethyl-1*H*-pyrrole] was synthesized as previously reported (*37*).

Reagent **c** was prepared according to Scheme 1.

*1-Oxyl-3-(1-bromoethyl)-2,5-dihydro-2,2,5,5-tetramethyl-1H-pyrrole (**2**).* To a stirred solution of 1-oxyl-3-(2-hydroxyethyl)-2,5-dihydro-2,2,5,5-tetramethyl-1*H*-pyrrole (**1**) (920 mg, 5.0 mmol, prepared as described in ref *38*) and Et_3N (555 mg, 5.5 mmol) in CH_2Cl_2 (30 mL) was added methanesulfonyl chloride (920 mg, 5.5 mmol) dropwise at 0 °C. The mixture was stirred at room temperature for 1 h.

Scheme 1

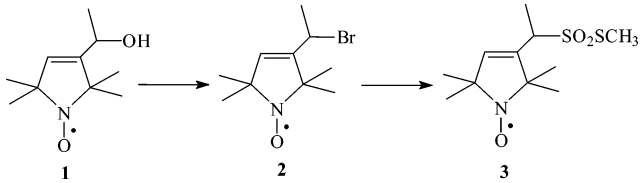

The organic phase was washed with brine (10 mL), separated, dried ($MgSO_4$), filtered, and evaporated to yield the corresponding mesylate. The crude mesylate and LiBr (434 mg, 5.0 mmol) were stirred and refluxed in acetone (20 mL) for 1 h. Acetone was evaporated, and the residue was dissolved in methylene dichloride (20 mL) and washed with brine (15 mL). The organic phase was dried, filtered, evaporated, and purified with flash column chromatography on silica gel (hexane/Et_2O) to give 1-oxyl-3-(1-bromoethyl)-2,5-dihydro-2,2,5,5-tetramethyl-1*H*-pyrrole (**2**) as a deep yellow oil: 890 mg (72%). Anal. Calcd for $C_{10}H_{17}BrNO$ (247.15): C, 48.60;

H, 6.93; N, 5.67; Br, 32.33. Found: C, 48.50; H, 7.10; N, 5.50; Br, 32.50. MS *m*/*z* (%): 248/246 (M^+, 10), 218/216 (4), 167 (19), 152 (84), 137 (100).

*1-Oxyl-3-(1-methanesulfonylthioethyl)-2,5-dihydro-2,2,5,5-tetramethyl-1H-pyrrole (**3**).* The above bromide **2** (247 mg, 1.0 mmol) and $NaSSO_2CH_3$ (202 mg, 1.5 mmol) in aqueous acetone (8:2) (10 mL) was cautiously heated to 50 °C, and the mixture was monitored by TLC. After consumption of starting material (30 min), the solvent was removed by evaporation, and the residue was extracted with $CHCl_3$ (2 × 30 mL). The organic phase was separated, dried ($MgSO_4$), filtered, and evaporated, and the residue was purified by flash chromatography on silica gel (hexane/ethyl acetate) to yield the title compound **3** as an orange solid: 181 mg (65%); mp 116 °C. Anal. Calcd for $C_{11}H_{20}NO_3S_2$ (278.40): C, 47.46; H, 7.24; N, 5.03; S, 23.03. Found: C, 47.70; H, 7.10; N, 5.20; S, 23.30. MS *m*/*z* (%): 278 (M^+, 21), 264 (8), 248 (4), 169 (100), 152 (80).

Labeling of 4-Thiouridine Derivatives. RNA containing singly substituted 4-thiouridine (1−50 μmol in 100 μL) was treated for 30 min with 100 μM DTT in buffer A at room temperature. The reaction mix was then loaded onto a PD-10 column (Amersham Biosciences) and eluted with buffer A. Fractions containing the RNA (∼2 mL) were reacted directly with the appropriate nitroxide reagent or MMTS (Toronto Research Chemicals, North York, Ontario, Canada) (final concentration 100 μM). After incubation at room temperature overnight, the excess reagent was removed by first passing it through a PD-10 column, followed by extensive washing using an Ultrafree 0.5 centrifugal filter (Millipore, Inc.). Labeled RNAs were stored in water at −20 °C to minimize the detachment of spin label from RNA due to the labile nature of the disulfide bond on the uridine heterocycle. Under conditions reported here, the labeled RNA can be stored at least 4 weeks, and dissociation of the label during room temperature measurement was slow (<1% for up to 6 h).

For MMTS, the degree of labeling was monitored via the quenching of the 4-thio-U absorbance peak at 335 nm. For spin label modifications, the percentage of labeling was estimated by comparing the concentration of the attached nitroxide to that of the RNA. RNA concentration was measured by its absorbance at 260 nm and calculated using an extinction coefficient of 248 966 M^{-1} cm^{-1}. The concentration of nitroxide was determined by comparing the total number of spins in the labeled RNA sample with that of a TEMPOL standard. In each case, the number of spins in the sample was determined by double integration of the EPR spectrum.

Thermodynamic Analyses of Labeled RNA. Thermal denaturation of RNA was carried out in a DU800 UV−vis spectrometer (Beckman Coulter, Fullerton, CA). RNA (0.7−3 μM in 380 μL) was dissolved in a buffer containing 50 mM sodium phosphate (pH 7.0) and 0.5 mM EDTA. The temperature was increased from 25 to 90 °C at a rate of 0.5 °C/min. Absorbance at 260 nm was recorded at every 0.5 °C. For labeled RNAs, comparison of either the absorbance or the EPR signals showed that the label remains attached to the RNA after thermal melting.

Thermodynamic data for the transition between the hairpin and the single-stranded form of RNA were calculated using the two-state model as described (*39*). Briefly, the fraction of single-stranded RNA (α) was calculated by taking the ratio at each temperature of the height between the experimental curve and the lower baseline and the height between the lower and the upper baseline. The temperature at which α = 0.5 is the melting temperature (T_m). The van't Hoff transition enthalpy and entropy were calculated as

$$\Delta H_{VH} = 4RT_m^2\left(\frac{\partial\alpha}{\partial T}\right)_{T=T_m} \quad (1)$$

$$\Delta S_{VH} = \Delta H_{VH}/T_m \quad (2)$$

Values of the free energy of transition at 37 °C were calculated as

$$\Delta G°_{37°C} = \Delta H_{VH} - 310\Delta S_{VH} \quad (3)$$

EPR Spectroscopy. EPR spectra were obtained in a Varian E-109 EPR spectrometer as described (*31*). Measurements were carried out with 30−100 μM labeled TLR. All spectra reported were obtained in 500 mM NaCl and 50 mM MOPS, pH 6.6, at room temperature. Measurements were carried out in 33.8% (w/v) sucrose to minimize effects due to tumbling of the entire molecule. Spectra were baseline corrected and normalized to a fixed number of spins. Signals from a small amount of free spin label (<1%) were subtracted (*40*). Values of the central line width and second moment were measured on the corrected spectra (*41*). Simulations of nitroxide spectra were carried out using the MOMD program developed by Freed and co-workers (*42*).

A rough estimate of the rotational correlation time (τ_R) for TLR, assuming a spherical shape, was made according to (*43*)

$$\tau_R = \frac{V_h\eta}{kT} \quad (4)$$

where V_h is the hydrated volume, η is the viscosity of the solution, k is the Boltzmann constant, and T (=293 K) is the absolute temperature. The hydrated volume was calculated as (*43*)

$$V_h = \frac{M}{N_0}(\overline{V_2} + \delta_1\overline{V_1}) \quad (5)$$

where M is the molecular weight (M = 7554.5 for TLR labeled with Rb), N_0 is Avogadro's number, $\overline{V_2}$ and $\overline{V_1}$ are the partial specific volumes of RNA and water, respectively, and δ_1 is the hydration factor. With values for $\overline{V_2}$, $\overline{V_1}$, and δ_1 of 0.50 cm^3 g^{-1}, 1.0 cm^3 g^{-1}, and 0.84, respectively (*43*), the rotational correlation time is estimated to be ≈16.6 ns at $\eta \approx 4$ cP. Correction for a nonspherical shape based on actual TLR dimensions was <5% (*43*).

NMR Spectroscopy. NMR spectra were acquired at 500 MHz on a Bruker DRX spectrometer. One-dimensional proton spectra were acquired at 278 K on samples that were 0.5−1.0 mM RNA strand, 100 mM NaCl, 10 mM sodium phosphate, pH 6.6, and 95% H_2O/5% D_2O. Two-dimensional NOESY spectra were acquired as described (*35*).

RESULTS

4-Thiouridine Labeling Scheme. Six uridine sites within TLR were singly substituted with 4-thiouridine (Figure 1B)

and modified with methanethiosulfonate derivatives (Figure 1A). In the following paragraphs, the labeled TLR RNA will be identified by specifying the base position and the spin label. For example, 4-thio-U19Ra-TLR is the TLR molecule with label Ra at position 19.

Upon reaction of the substituted 4-thiouridine with a methanethiosulfonate reagent to form a disulfide bond, the characteristic 4-thio-U absorbance (λ_{max} ~335 nm) was replaced by a new peak with λ_{max} ~310 nm that represents the adduct (Figure 1C). This is consistent with previous reports (*44*) and provides an independent method to monitor the progress of the labeling reaction. The reactions of the 4-thiouridine derivatives with methanethiosulfonate reagents were essentially quantitative, with the measured labeling efficiency ranging from 85% to 100%, and no RNA degradation was detected by HPLC or gel electrophoresis.

Perturbation to RNA Structure. Disruption of RNA structure due to the 4-thio-U labeling could arise from two sources. First, derivatization of the 4-thio-U to form a disulfide bond is expected to result in loss of the imino proton. At positions U5 and U16, this will also result in the loss of a hydrogen bond involved in base pairing and might lead to significant structural perturbations. In addition, the nitroxide group of the spin label might interact with the RNA and either stabilize or destabilize the structure.

Structural perturbation due to the loss of the N3 proton is the greatest concern, and the degree of perturbation was assessed by three methods. First, NMR studies were carried out to probe the effect of 4-thio-U substitution and subsequent derivatization to form a disulfide. The U16 base was selected for detailed study. Comparison of the imino region of the 1D NMR spectra of TLR and 4-thio-U16-TLR reveals no difference in the 5′/3′ stem (G2C3C4/G20G21C22) and the UUCG loop region (Figure 2). The imino proton resonance of 4-thio-U16 is present, indicating that base pairing and H-bonding at position 16 are maintained. Chemical shift changes relative to TLR are observed at G15 and U17, the neighboring bases of 4-thio-U16. This is consistent with previous reports on 4-thio-U-modified RNAs (*45*). Collectively, the data indicate that the 4-thio-U substitution itself does not significantly alter the structure of TLR.

NMR studies were then carried out on 4-thio-U16-TLR modified with the MMTS reagent. MMTS forms the same disulfide bond with the 4-thio-U as the spin label reagents but replaces the nitroxide moiety with a simple methyl group. With this derivative, referred to as 4-thio-U16M-TLR, it is possible to obtain high-resolution NMR spectra and to eliminate possible effects of the more bulky nitroxide ring, thereby isolating effects due to loss of the imino proton. The NMR spectrum of 4-thio-U16M-TLR is shown in Figure 2. As anticipated, the resonance for the imino proton of U16 is missing. The assignment of imino proton resonances of G2, G8, G21, G20, U11, and G14 can be made by comparison with the spectrum of 4-thio-U16-TLR, because shifts are either small (G8, U11, G14) or absent (G2, G21, G20). Assignments for G2, G20, and G21 were confirmed by the 2D NOESY spectrum (not shown). The presence of the G2, G20, G21, U11,and G14 resonances clearly demonstrates that the wild-type structure in the 5′/3′ stem and the UUCG loop are preserved.

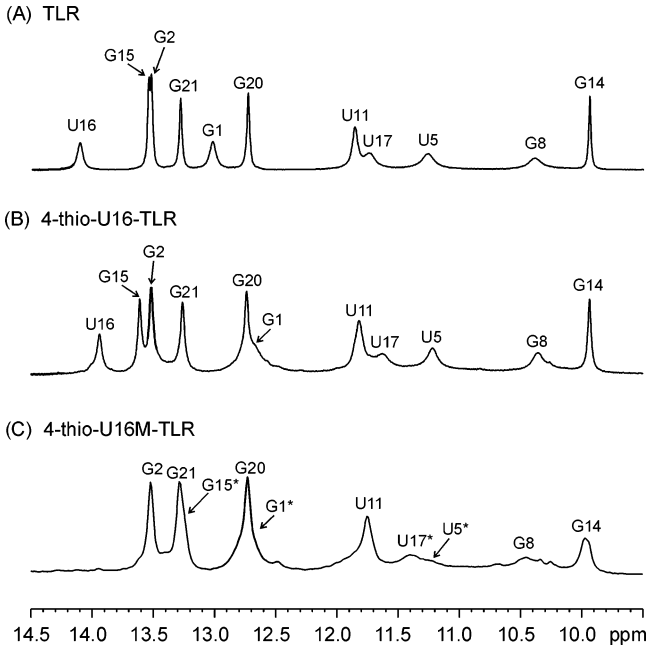

FIGURE 2: One-dimensional NMR spectra for the imino region. (A) TLR. Resonance peaks were assigned on the basis of 2D NOESY measurements and previously reported assignments (*35*). (B) 4-Thio-U16-TLR. Compared to TLR, the resonance positions of U16, G15, and U17 were slightly changed due to the 4-thio-U substitution. The G1 resonance was altered due to the presence of a 5′-hydroxyl group instead of a 5′-triphosphate. (C) 4-Thio-U16M-TLR. The asterisks indicate tentative assignments. The presence of an imino proton resonance overlapping with that of G2 was confirmed in the 2D spectrum. This was tentatively assigned to G15.

Assignments for the imino proton resonances of G15 and U17, the neighboring bases of U16, are uncertain because of significant chemical shifts and loss of sequential imino−imino connectivities in the NOESY spectrum due to the lack of the U16 imino proton. Tentative assignments are based on observed (weak) NOEs to the aromatic/aminos. The chemical shift changes for G15 and to a lesser extent U17 are consistent with changes in ring current shifts from the stacked 4-thio-U16M-TLR due to changes in its electronic structure relative to 4-thio-U16-TLR. Atomic level structural information in the region around the labeled base is not available without $^{13}C,^{15}N$-labeled RNA for additional NMR data on which to base assignments. Of the assignable resonance lines, those of G8 and G14 are clearly broadened relative to 4-thio-U16-TLR. Irrespective of the assignments, there is also broadening of the resonances in the region corresponding to U5 and U17. A likely origin of this effect is discussed below.

The above NMR data are consistent with the 4-thio-U16M-TLR base being stacked in the TLR following chemical modification. To further address this question, site-specific hyperchromicity measurements were carried out. Comparison of UV−vis spectra of 4-thio-U16M-TLR at 25 and 85 °C (above the melting point) reveals an 11% and 17% increase in absorbance at 260 and 310 nm, respectively. The increase at 260 nm that reports the melting of the entire molecule is similar to that of the unmodified 4-thio-U16-TLR under the same conditions (12%). Because the absorbance at 310 nm is specific to the labeled base (Figure 1C), the 310 nm hyperchromicity represents unstacking of labeled base (U16)

Table 1: Thermodynamic Data for TLR Molecules

RNA	T_m[a] (°C)	ΔT_m[b] (°C)	ΔH_{VH}[a] (kcal/mol)	$\Delta G°_{37°C}$[a] (kcal/mol)	$\Delta\Delta G°_{37°C}$[c] (kcal/mol)
TLR	64.9 ± 0.2	NA[d]	66.8 ± 2.3	5.47 ± 0.15	NA[d]
4-thio-U5-TLR	63.6 ± 0.1	−1.3	56.1 ± 2.9	4.42 ± 0.23	−1.05
4-thio-U5Rb-TLR	62.9 ± 0.5	−2.0	59.0 ± 1.3	4.52 ± 0.17	−0.95
4-thio-U11-TLR	62.4 ± 0.2	−2.5	60.3 ± 0.3	4.56 ± 0.1	−0.91
4-thio-U11Rb-TLR	62.7 ± 0.2	−2.2	63.3 ± 2.4	4.81 ± 0.23	−0.66
4-thio-U12-TLR	64.2 ± 0.2	−0.7	67.9 ± 1.1	5.48 ± 0.04	0.01
4-thio-U12Rb-TLR	63.5 ± 0.4	−1.4	71.5 ± 1.3	5.59 ± 0.02	0.12
4-thio-U16-TLR	64.3 ± 0.5	−0.6	62.4 ± 2.9	4.98 ± 0.19	−0.49
4-thio-U16M-TLR	63.5 ± 0.8	−1.4	49.0 ± 4.4	3.98 ± 0.44	−1.49
4-thio-U16Rb-TLR	63.0 ± 0.4	−1.9	62.2 ± 0.5	4.78 ± 0.10	−0.69
4-thio-U17-TLR	64.5 ± 0.2	−0.4	64.9 ± 1.3	5.28 ± 0.14	−0.19
4-thio-U17Rb-TLR	64.2 ± 0.9	−0.7	67.5 ± 7.2	5.42 ± 0.74	−0.05
4-thio-U19-TLR	63.7 ± 0.1	−1.2	66.3 ± 2.4	5.25 ± 0.21	−0.22
4-thio-U19Rb-TLR	64.7 ± 0.5	−0.2	68.1 ± 1.2	5.54 ± 0.19	0.07

[a] Errors were calculated from at least two independent measurements. [b] $\Delta T_m = T_m - T_m$(TLR). [c] $\Delta\Delta G°_{37°C} = \Delta G°_{37°C} - \Delta G°_{37°C}$(TLR). [d] Not applicable.

upon melting of the molecule, indicating that the labeled U16 base is stacked in 4-thio-U16M-TLR below the melting point.

The third measure of the perturbation due to 4-thio-U labeling is the melting temperature (T_m). As listed in Table 1, the 4-thio-U*x*-TLR's have small melting point depressions of ≤1.3 °C (relative to TLR), except for 4-thio-U11-TLR, which has the largest depression observed for any of the TLR analogues investigated (−2.5 °C). Even for this site, the decrease in free energy $\Delta G°_{37°C}$ is less than 1.0 kcal/mol. This small effect of 4-thio-U substitutions in RNA is consistent with a previous report (*45*).

Table 1 also shows the effect of chemical modification of the 4-thio-U on thermodynamic parameters. Of particular interest are the TLR molecules with 4-thio-U substitutions at U5 and U16, the positions where base pair hydrogen bonding is compromised following disulfide formation at the 4-thio group. The melting point of 4-thio-U16M-TLR should reflect any destabilization due to the loss of a hydrogen bond in the corresponding base pair. As shown in Table 1, the melting point depression relative to TLR is modest at −1.4 °C, only 0.7 °C less than the melting point of 4-thio-U16-TLR itself where the U16 is known to be stacked. This result strongly supports the above conclusion that, upon chemical modification at U16, one hydrogen bond is lost, yet the base remains stacked within the helix.

Table 1 also includes thermodynamic data on all of the spin-labeled TLR molecules investigated in this study. Compared to TLR, all spin-labeled RNAs showed small decreases in T_m (≤2.2 °C) and $\Delta G°_{37°C}$ (≤1.0 kcal/mol). Moreover, variations of $\Delta G°_{37°C}$ between 4-thioU*x*-TLR and 4-thio-U*x*Rb-TLR were between −0.34 and 0.25 kcal/mol, indicating that the nitroxide group does not cause significant perturbation to the RNA structure.

Collectively, the data indicate that neither 4-thio-U substitution nor subsequence modification with the nitroxide spin label causes significant disruption of the structure of the TLR RNA.

Motion of Ra and Rb at U16. The EPR spectra of TLR with spin labels Ra and Rb in 33.8% sucrose solution (w/v) are shown in Figure 3. The high viscosity of the sucrose solution ($\eta \approx 4$ cP) reduces the overall tumbling rate of the receptor to the point where it has only minor effects on the

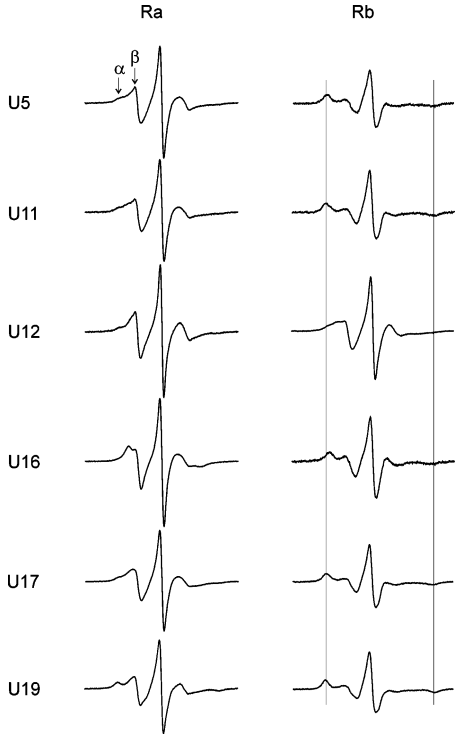

FIGURE 3: EPR spectra of Ra (left column) and Rb (right column) at various sites in TLR. Spectra were obtained in 33.8% (w/v) sucrose to limit the influence of the overall tumbling of the molecule. Arrows in the spectrum of 4-thio-U5Ra-TLR identify two distinct components (α and β). In the Rb series, vertical lines that mark the outer hyperfine extrema in the 4-thio-U5Rb-TLR spectrum are provided to aid in comparison of the spectra at different sites. The scan width is 100 G.

X-band EPR spectra ($\tau_R \approx 16.6$ ns). Thus, the spectra reflect internal motions of the label and motions of the base to which it is attached. It has been reported that sucrose alters the local dynamics of proteins (*46*), presumably mediated by changes in osmolarity. However, when sucrose was substituted with Ficoll, a polymer that has little effect on osmolarity, no changes in EPR spectra were observed at the same effective viscosity.

The spectra of Ra at positions 5, 11, 12, 17, and 19 are complex, having at least two components, identified in Figure 3 as α and β for 4-thio-U5Ra-TLR, corresponding to

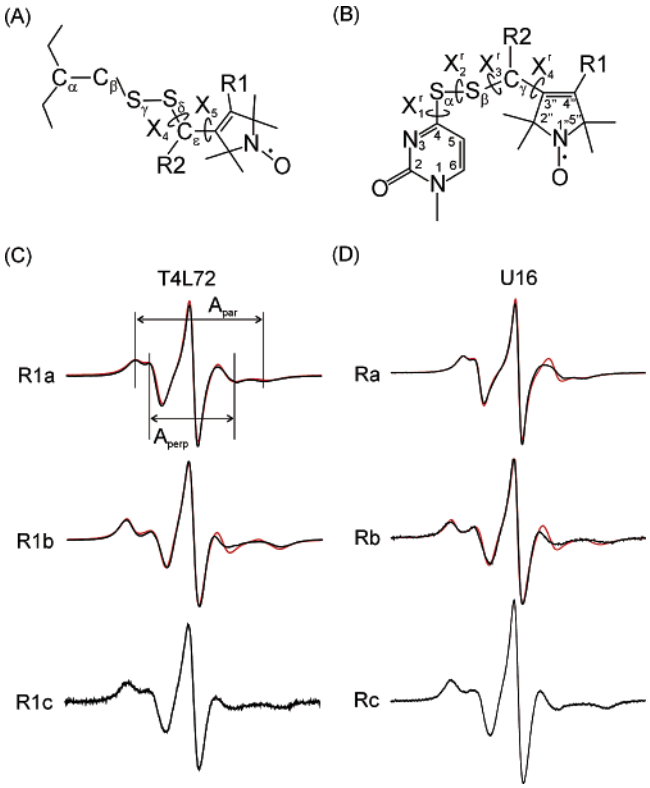

FIGURE 4: Structures of spin labels and the corresponding EPR spectra in T4L and TLR. (A) Structure of the R1*x* series of side chains employed in proteins. These side chains are generated when reagents R*x* (Figure 1A) react with cysteine residues. X_4 and X_5 are the dihedral angles of the two bonds adjacent to the nitroxide ring. (B) Structure of the R*x* series of spin labels, showing the designation of the various atoms and dihedral angles. (C) EPR spectra of R1a, R1b, and R1c at helix surface site 72 in T4L (black traces). Spectra of R1a and R1b were taken from ref *22*. Dr. Ned van Eps provided the spectrum of R1c (unpublished data). Spectra simulated according to the MOMD model for R1a and R1b are shown in red. The order parameters for the simulated spectra of R1a and R1b are 0.47 and 0.81, respectively, and the diffusion tilt angle (β_D) is 36° (*22*). The vertical lines in the spectrum of R1a identify the outer (A_{par}) and inner (A_{perp}) hyperfine extrema. (D) EPR spectra of Ra, Rb, and Rc at site U16 in the TLR (black traces). Also shown for Ra and Rb are spectra simulated with the MOMD model (red traces). For Ra and Rb, the order parameters for the simulated spectra are 0.46 and 0.82, respectively; the diffusion tilt angles (β_D) are 36°. For both simulated spectra, the *g* and *A* tensor values were $g_z = 2.0023$, $g_x = 2.0076$, $g_y = 2.0050$, $A_z = 37.2$, $A_x = 7.5$, and $A_y = 5.9$. The rotational diffusion tensor values were $R_x = 1.45$ ns, $R_y = 1.42$ ns, and $R_z = 1.24$ ns.

relatively immobile (α) and mobile (*β*) spin populations. Such spectra arise from interactions of the nitroxide with the local environment that modulate the mobility (*41*, *47*). On the other hand, the distinctive spectrum of 4-thio-U16Ra-TLR is characteristic of a single dynamic population of nitroxides having an anisotropic motion. This line shape has been observed, and its molecular origin studied in detail, for spin-labeled lipids in bilayers (*48*) and for the nitroxide side chain designated R1a at helix surface sites in proteins (*22*, *41*). Figure 4A shows the structure of the R1*x* series of side chains used in proteins (*22*). The R1a side chain (R1 = R2 = H) is introduced by reaction of the methanethiosulfonate reagent **a** with a cysteine residue. With the exception of the C_β carbon atom, R1a has the same structure as the spin label Ra on uridine (compare panels A and B of Figure 4).

For comparative purposes, panels C and D of Figure 4 (top panels) show the EPR spectra of R1a at helix surface site 72 in T4L (T4L72R1a) and Ra at U16, respectively. The positions of well-resolved hyperfine extrema in the spectrum of T4L72R1a, characteristic of axial anisotropic motion, are indicated by vertical lines in Figure 4C (top panel), and the splittings are labeled A_{par} and $A_{perp.}$ For helix surface sites, the R1a side chain has no interaction with nearest neighbors (by definition), and the motion is determined by bond rotations within the side chain and fluctuations of the backbone structure. At site 72 in T4L, backbone motions are expected to be minor (*22*). Previous analyses suggested that the anisotropic motion of R1a at helix surface sites arises predominantly from motion about the two terminal bonds in the side chain, i.e., torsional oscillations of the X_4, X_5 dihedral angles (Figure 4A) (*22*). X-ray crystallographic data (*49*) indicate that motions about bonds more proximal to the backbone (X_1-X_3) are damped by interaction of the disulfide with main chain atoms.

The similarity of the spectra for 4-thio-U16Ra-TLR and T4L72R1a (Figure 4C,D) indicated that the motion of the nitroxide must be similar in the two cases. Given the similarity of the structures for the two labels, it is reasonable to infer that the motion of 4-thio-U16Ra-TLR may also be dominated by motion about the two terminal bonds in the label, namely, X_3^r and X_4^r (Figure 4B). This model can be tested using spin label analogues with specifically hindered internal motions, as was done for R1a at helix surface sites (*22*). For example, a $-CH_3$ substituent introduced at the 4″ position of the nitroxide ring in R1a (to produce the new side chain R1b) has a steric clash with S_δ that reduces the amplitude of torsional oscillations about the terminal dihedral, X_5 (Figure 4A). This produces a dramatic reduction in nitroxide mobility only if the overall motion has dominant contributions from the X_5 oscillations, and this is the case for R1a at helical sites in proteins, as mentioned above. The effect is illustrated in Figure 4C for R1a and R1b at site 72 in T4L, where the large increase in the apparent hyperfine coupling (A_{par}) due to the 4″-CH_3 indicates reduced mobility (*22*). Panels C and D of Figure 4 show the striking similarity of the effects of the 4″-CH_3 substituents in both 4-thio-U16Rb-TLR and T4L72R1b in reducing the nitroxide motion. This supports the contention that the internal motion of 4-thio-U16Rb-TLR has dominant contributions from torsional oscillations about X_3^r and X_4^r, while motion about X_1^r and X_2^r must be constrained. As will be discussed below, molecular models suggest possible origins for the constraints on motions of X_1^r and X_2^r.

Further support for the "X_3^r/X_4^r" model for Ra motion at U16 in the TLR comes from fitting of the experimental spectra to the microscopic order/macroscopic disorder (MOMD) model developed by Freed and co-workers (*42*). This model characterizes the spectra from anisotropic motions in terms of an order parameter and diffusion rates about three mutually perpendicular axes and has been previously shown to accurately account for the experimental spectra of R1a and R1b at site 72 in T4L (Figure 4C, top and center panels, red traces) (*22*). Remarkably, the spectrum of 4-thio-U16Ra-TLR can be fit with essentially the same parameter set as for T4L72R1a but with slightly higher diffusion rates (Figure 4D, top panel, red trace). Moreover, the effect of the 4″-CH_3 can be accounted for by a simple increase in the

Table 2: Spectral Parameters for Rb-Labeled TLR Molecules

RNA	$(\Delta H_{pp})^{-1}$ (G^{-1})	$(\langle H_2 \rangle)^{-1}$ ($\times 10^{-3}$ G^{-2})	$2A_{par}'$ (G)
4-thio-U5Rb-TLR	0.209	3.70	66.15
4-thio-U11Rb-TLR	0.203	3.68	66.39
4-thio-U12Rb-TLR	0.359	4.17	NA
4-thio-U16Rb-TLR	0.274	3.89	62.19
4-thio-U17Rb-TLR	0.181	3.66	66.68
4-thio-U19Rb-TLR	0.173	3.59	68.34

order parameter, just as for the labels at T4L72 (Figure 4C,D, center panels, red traces).

It could be argued that the effect of the 4″-CH_3 in 4-thio-U16Rb-TLR arises from interactions of the methyl group with the environment, rather than from steric interactions within the side chain. This can be tested using the derivatives R1c and Rc in the protein and RNA, respectively. Molecular models indicate that the 4″-CH_3 in R1b and Rb and the C_ϵ-CH_3 of R1c or C_γ-CH_3 of Rc have similar steric clashes that reduce the internal motion of the nitroxide by restricting the amplitudes of oscillations of X_4/X_5 or X_3^r/X_4^r (not shown). In the case of the 4″-CH_3, the steric clash is with a sulfur of the disulfide, while in the C_ϵ-CH_3 or C_γ-CH_3 it is between the methyl group and the 2,2,5,5-methyl groups in the nitroxide ring. Thus, repositioning of the methyl group is expected to preserve the restriction on bond rotations but would alter any local interactions that occur with the environment. As shown in Figure 4C (center and lower panels), the spectra of R1b and R1c at T4L72, where there are no local interactions, are essentially identical. This supports the assertion that the steric effects of the methyl groups at the two positions are indeed similar. The fact that a similar result is found for Rb and Rc at U16 (Figure 4D) strongly argues against possible interactions of the 4″-CH_3 with the RNA environment at this site.

Comparative Mobility of Rb. For each site investigated, with the exception of U12, the effect of the 4″-CH_3 substituent is to dramatically reduce the mobility (Figure 3) of the nitroxide to produce a state similar to that of 4-thio-U16Rb-TLR, as would be anticipated if the X_3^r/X_4^r model were applicable to these sites on the RNA. At U12, the effect of the substituent is also to reduce the mobility, but to a much lesser degree than at the other sites, suggesting that other dynamic modes are adding to the X_3^r/X_4^r internal bond motions.

To provide a semiquantitative relative measure of the mobility of nitroxides at different sites in proteins, the values of the inverse central line width $[(\Delta H_{pp})^{-1}]$ and of the inverse second moment $[(\langle H_2 \rangle)^{-1}]$ have been utilized (*22*, *41*). For these measures, larger values of $(\Delta H_{pp})^{-1}$ and $(\langle H_2 \rangle)^{-1}$ represent higher mobility. In spectra corresponding to nitroxide motion in the slow motional regime, or where the motion is highly ordered, the splitting between the outer hyperfine extrema (A_{par}) provides another measurement of the nitroxide mobility, with larger A_{par} indicating lower mobility. It should be noted that a full description of the nitroxide motion requires assessment of both the rate and the amplitude (order) of the motion. In the semiquantitative approach used here, "mobility", as measured by $(\Delta H_{pp})^{-1}$ and $(\langle H_2 \rangle)^{-1}$, is a function of both rate and order, and these are not distinguished.

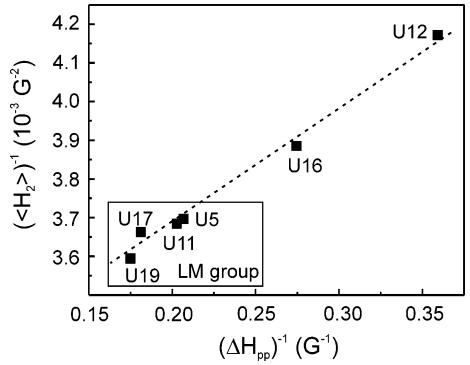

FIGURE 5: Correlation of the inverse central line width $(\Delta H_{pp})^{-1}$ and the inverse second moment $(\langle H_2 \rangle)^{-1}$ for Rb on TLR. The box indicates the group of sites designated as low mobility.

For the Rb label, values of $(\Delta H_{pp})^{-1}$ and $(\langle H_2 \rangle)^{-1}$ are shown in Table 2. In a plot of $(\Delta H_{pp})^{-1}$ vs $(\langle H_2 \rangle)^{-1}$, the data points fall on a straight line (Figure 5), indicating that $(\Delta H_{pp})^{-1}$ and $(\langle H_2 \rangle)^{-1}$ are equivalent measures of mobility. In addition, the mobility trend reported by $(\Delta H_{pp})^{-1}$ and $(\langle H_2 \rangle)^{-1}$ is reflected in that of the A_{par} values (Table 2). Thus, $(\Delta H_{pp})^{-1}$, $(\langle H_2 \rangle)^{-1}$, or A_{par} can be used to characterize the mobility of Rb in RNA.

As mentioned above, the spectra of Ra at sites other than U16 reflect at least two dynamical populations of the label arising from interactions with the local environment. The relative proportion of the components and their mobilities contain detailed information on the environment and the dynamic modes of the local structure. However, the simple measures of $(\Delta H_{pp})^{-1}$ and $(\langle H_2 \rangle)^{-1}$ are not equivalent, because $(\Delta H_{pp})^{-1}$ is biased toward the most mobile component, while $(\langle H_2 \rangle)^{-1}$ is biased toward the most immobile component. In addition, hyperfine extrema are not generally well resolved, and A_{par} cannot be employed.

Correlation of Rb Mobility with RNA Base Dynamics and Structure. On the mobility plot of Rb in TLR (Figure 5), the six labeling positions can be grouped into three classes: high mobility (U12), intermediate mobility (U16), and low mobility (U5, U11, U17, and U19). The spectrum of 4-thio-U12Rb-TLR reflects a much higher mobility than that for any of the other sites, with a relatively narrow central resonance line, no resolved hyperfine A_{par} splitting, and the highest values of $(\Delta H_{pp})^{-1}$ and $(\langle H_2 \rangle)^{-1}$ (Figure 3, Table 2). This high mobility of the spin label likely originates from RNA base motion. U12 is located within the UUCG terminal loop that caps the TLR molecule, and NMR studies have shown that this base has no structural constraints and its conformation cannot be defined (*50*). This indicates that U12 is highly dynamic, a result that correlates well with the observed EPR spectrum.

The four sites U11, U17, U5, and U19 (the low-mobility group) show relatively immobilized EPR spectra, having well-resolved outer hyperfine extrema and low values of $(\Delta H_{pp})^{-1}$ and $(\langle H_2 \rangle)^{-1}$ for the Rb label (Figure 3, Table 2). In Figure 5, they cluster in the region of lowest mobility. In the TLR structure, bases within the low-mobility group are all hydrogen bonded and stacked within the helix (*35*): U17 is involved in a U/G pair, U5 and U19 form an unusual U/U pair, and U11 forms a bifurcated hydrogen bond with G14 and stacks on the adjacent C/G pair (*50*). Moreover, ^{15}N relaxation studies show that U11 has a high order parameter

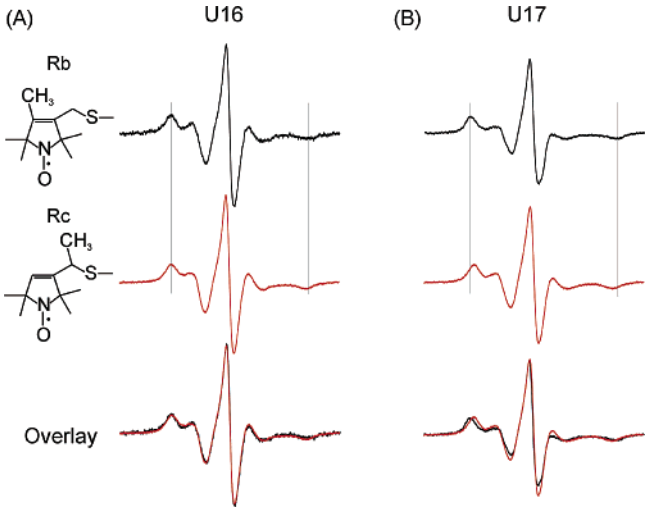

FIGURE 6: Interaction between the nitroxide moiety and RNA. (A) EPR spectra of 4-thio-U16Rb-TLR (black) and 4-thio-U16Rc-TLR (red), reproduced from Figure 3 for comparison. The superposition of the two spectra shows their near identity. (B) EPR spectra of 4-thio-U17Rb-TLR (black) and 4-thio-U17Rc-TLR (red). The superposition reveals that the hyperfine splitting, A_{par}, is significantly smaller in the spectrum of Rc, indicating that it is more mobile than Rb.

and is as rigid as those bases that are paired within the RNA duplex (*3*). For this group of RNA bases, base motion is highly ordered with small amplitude. The rigid EPR spectra at these positions correlate well with the low mobility of the bases and provide further support that nitroxide labeling does not disrupt the structure of the TLR.

However, the nitroxide mobility in the low-mobility group is significantly lower than that of U16, which in the TLR structure participates in a standard Watson−Crick base pair embedded in the middle of the helix (*35*). As nitroxide mobility at U16 reflects primarily the X_3^r/X_4^r internal bond motions that are free from local RNA contacts, a possible origin for reduced mobility in the low-mobility group is that the nitroxides have interactions with the local RNA environment that are absent in 4-thio-U16Rb-TLR. For instance, the nitroxide at U19 is the most immobilized. The A_{par} measured from the 4-thio-U19Rb-TLR spectrum is 68.3 G, which corresponds to correlation time of ≈16.5 ns (*51*), very close to the calculated rotational correlation time for the entire TLR molecule (16.6 ns; Materials and Methods). This indicates that at U19 the nitroxide is essentially immobilized relative to the molecule, a condition that clearly requires strong local interactions.

To examine possible origins of nitroxide ring interactions within the TLR structure, the spectrum of 4-thio-U17Rc-TLR was obtained and compared with 4-thio-U16Rc-TLR (Figure 6). Unlike the case for position U16, the spectrum of 4-thio-U17Rc-TLR is clearly more mobile than that of 4-thio-U17Rb-TLR, as judged by the center line width and A_{par} (Figure 6). Interestingly, the spectrum of 4-thio-U17Rc-TLR closely resembles that of 4-thio-U16Rc-TLR (Figure 6). Taken together, these data suggest that the 4″-CH_3 in 4-thio-U17Rc-TLR provides an additional restriction on the motion of the nitroxide ring. From modeling studies discussed below, this extra restriction is likely steric interaction between the methyl group and the phosphate backbone of the RNA.

DISCUSSION

Advantages and Limitations of the 4-Thiouridine Method for RNA Spin Labeling. The 4-thio-U RNA spin labeling scheme presented here parallels what has been developed for protein SDSL studies: The nitroxide is attached to the molecule of interest via a disulfide linkage, and the nitroxide mode of motion is similar between the RNAs and proteins. This implies that knowledge obtained in protein SDSL studies, and the vast array of spin label derivatives developed, might be applied to some degree in RNA SDSL studies. This should greatly accelerate the development of RNA SDSL.

The degree of perturbation is always an issue for techniques such as SDSL, which employ external reporter groups. In the TLR system, thermal denaturation analyses, site-specific hyperchromicity measurements, and NMR studies all indicate that the 4-thio-U labeling does not alter the basic RNA fold at the level of structural resolution currently sought in the SDSL experiment, namely, the state of stacking of the RNA bases. Consistent with this conclusion, the dynamics of the nitroxide at all sites investigated can be interpreted in a straightforward manner in terms of the known structural and dynamical information on the native TLR molecule.

As noted above, the 1D NMR spectrum of 4-thio-U16M-TLR showed an increase in line width and small shifts for the assignable imino proton resonances of G8 and G14 relative to those in 4-thio-U16-TLR (Figure 2). It is likely that this effect arises from exchange on the microsecond to millisecond time scale between two (or more) conformations of the bases that have significant differences in chemical shift of the imino proton. Because the shifts that accompany the broadening are small, the dominant conformation must be similar to that in 4-thio-U16-TLR (*52*). On the EPR time scale, the proposed base exchange is slow, and multiple conformations would be detected as separate populations in the EPR spectrum of the spin-labeled U16 base. As shown in Figure 4, the EPR spectra of the spin-labeled U16 base can be accurately simulated as a single homogeneous spin population. However, a spin population less than about 10% would not be readily detected, and this result is compatible with the interpretation of the NMR resonance broadening given above. Within the context of this model, the NMR line broadening has little consequence for interpretation of the EPR spectra. The origin of the multiple populations is a matter of speculation, but one possibility is slight chemical degradation of the synthetic RNA during NMR studies. Indeed, analysis of the NMR sample shows some degradation at the level of a few percent (data not shown).

Among the disadvantages of the 4-thiouridine scheme is the limitation to uridine sites within RNA. Alternatively, other modified bases, such as 6-thio-G, may be exploited to expand the scope of available RNA labeling sites. Complementary to the 4-thiouridine scheme reported here, a method has recently been reported for attaching spin labels to the 2′-sugar positions in RNA, and it was shown that the dynamics of the nitroxide correlates with the RNA structure (*30*). In addition, a scheme for attaching nitroxides to the phosphorodiester backbone of RNA has been reported (*31*). Together, these methods provide a powerful set of tools for studying RNA dynamics and structure by SDSL.

Anisotropic Internal Motion of Rx Labels. Data presented above suggest a model for the internal motion of 4-thio-

U16Ra-TLR in which rotations of the X_1^r and X_2^r torsion angles are restricted, leading to an anisotropic motion of the nitroxide dominated by torsional oscillations of X_3^r and X_4^r. The absence of interaction of U16-labeled Ra with the local environment and the restricted X_1^r and X_2^r rotations would account for the striking similarity of the line shapes of 4-thio-U16Ra-TLR and R1a at helical surface sites in proteins. On the basis of the X_3^r/X_4^r model, a similar motional model, with the amplitude modulated by the methyl group, is expected for both Rb and Rc.

The restricted X_2^r motion is due to characteristics of the disulfide bond, where the preferred energy minimum configuration is $X_2^r = \pm 90°$ and the free energy of activation for the interconversion between the states is ~6.6−9 kcal/mol (*53*). Therefore, disulfide bond isomerization is too slow to contribute to the observed nitroxide motion (*54*), although limited torsional oscillations about X_2^r may contribute. The origin for the apparent restriction in X_1^r rotation is not clear. Whatever the origin, the X_1^r and X_2^r restrictions for the Ra label at U16 are apparently due to the interactions that occur within the spin-labeled base. If so, a restricted X_1^r and X_2^r rotation would be characteristic of any disulfide-linked spin label at 4-thiouridine, independent of position, although at highly constrained sites steric interactions could dictate alternative configurations of the label.

As for any labeling scheme where the label has internal modes of motion, the modes must be understood in order to distinguish effects of local interactions and base motions on the EPR spectrum. The simple motional model introduced here is a step in that direction. However, more data are required to establish a database relating the observed EPR spectra to RNA structural elements in order to critically evaluate the model.

Comparison of Ra, Rb, and Rc as Probes for Local RNA Structure and Dynamics. The EPR spectra of spin label Ra reflect both internal motion within the label and motion of the uridine base relative to the RNA molecule. As revealed by the presence of multiple components in the EPR spectra of Ra (Figure 3), the internal motion is modulated by interactions between the nitroxide label and RNA, making it a sensitive indicator for the difference in local RNA structure. On the other hand, labels Rb and Rc have restricted internal motion, making them more sensitive indicators for motion of the base to which they are attached. For these labels, the mobility is moved into a sufficiently low range that a second low-mobility state arising from a local interaction is not resolved as a second spectral component. In spectra of Rb and Rc, simple spectral parameters, such as $(\Delta H_{pp})^{-1}$, $(\langle H_2 \rangle)^{-1}$, and A_{par}, suffice as semiquantitative measures of probe mobility. Rb and Rc differ only in the position of a single methyl group, and at noninteracting sites in proteins and RNA, their internal motions, as judged by X-band EPR line shapes, are essentially identical (Figure 4C,D). This result is apparently due to similar effects from steric interactions of the methyl group within the label itself. However, at sites where interactions with the environment are possible, their motions can be quite different (Figure 6). For example, a direct interaction with the nitroxide ring might be strongly modulated by the 4″-CH_3 in Rb but not by the C_γ-CH_3 in Rc. Even if contacts between the C_γ-CH_3 and the RNA were made, the effects on ring motion would be minimized, because this interaction would not alter the dominant motions of X_3^r and X_4^r. Thus, the Rb, Rc pair may prove to be of general use in exploring features of the local environment in RNA and protein structures.

Correlation of Rb Mobility with RNA Structure and Dynamics. Data presented here reveal a direct correlation between Rb mobility and the structural state of the RNA base. In particular, all bases that are hydrogen bonded and stacked show lower mobility than U12, the structurally unrestricted base of the UUCG loop. This is expected on the basis of current knowledge of base dynamics. NMR studies of RNA base dynamics using hydrogen exchange showed that the lifetime of an RNA base in the paired state ranges from microseconds to minutes (*55*, *56*). Therefore, large amplitude motion of a paired base is very slow and will not contribute to the EPR spectrum of nitroxide, which is sensitive to motion in the 0.1−50 ns regime. On the other hand, for the structurally unrestricted U12 within the UUCG loop, the data revealed RNA base motion in the 0.1−50 ns regime that contributes significantly to the overall motion of nitroxide. This represents the first report of such RNA motion revealed via an experimental technique. It will be interesting to see whether motions in this regime are common among unrestricted RNA bases.

As discussed above, the R*x* labels at U16 apparently do not have interactions with the local environment, a result consistent with the molecular model for the site shown in Figure 7A. In this case, internal motions within the label and motions of the base itself determine the overall mobility of the nitroxide. Because U16 is apparently stacked within the RNA helix, base motions in the nanosecond regime are expected to be of relatively low amplitude. Moreover, in 4-thio-U16Rb-TLR, internal motions are constrained (but not eliminated) by the 4″-CH_3 substituent, and the label is enhanced for detecting changes in base motion. Within the context of this model, shifts toward *higher mobility* relative to the simple 4-thio-U16Rb-TLR reference state are assigned to contributions from base dynamics, while shifts toward *lower mobility* are assigned to contributions from direct RNA interactions. Thus, 4-thio-U12Rb-TLR, discussed above, is an example of the former, while members within the low-mobility group (U5, U11, U17, and U19) are examples of the latter.

It is of interest to consider possible origins of nitroxide/RNA interactions that distinguish the low-mobility group from U16. In helical regions of RNA, the spin label resides within the major groove, and the different geometry of the RNA groove in different sequences should lead to variable restrictions on the motion of the nitroxide moiety. Figure 7 shows the Rb label modeled onto the TLR structure at sites U5, U16, U17, and U19 (see legend for details). As mentioned above, the model of 4-thio-U16Rb-TLR clearly reveals an unrestrictive environment consistent with the rapid anisotropic motion and lack of interaction of the nitroxide (Figure 7A). On the other hand, it is not possible to find a conformation for 4-thio-U5Rb-TLR and 4-thio-U19Rb-TLR that eliminates all contact interactions of the nitroxide ring with the RNA backbone (Figure 7B,C), consistent with the lower mobility relative to 4-thio-U16Rb-TLR (Figure 3). This is particularly pronounced in the case of 4-thio-U19Rb-TLR, where the nitroxide is nearly completely buried within the RNA (Figure 7C), and the nitroxide has the lowest mobility in the low-mobility group (Figure 5). As mentioned above,

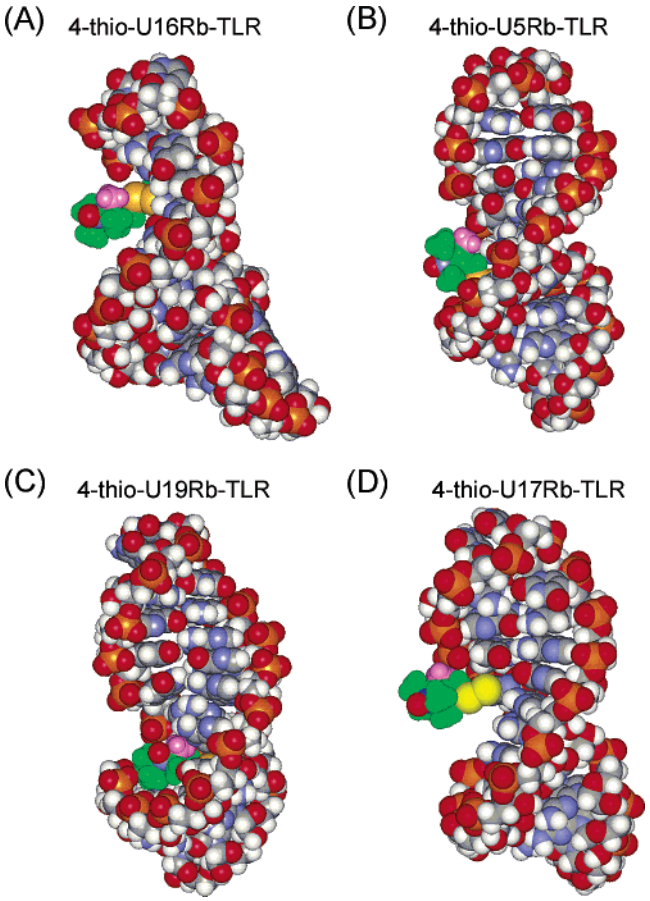

FIGURE 7: Structural models of the TLR RNA with Rb attached: (A) 4-thio-U16Rb-TLR; (B) 4-thio-U5Rb-TLR; (C) 4-thio-U19Rb-TLR; (D) 4-thio-U17Rb-TLR. The Rb label was modeled onto the solution structure of TLR [PDB code 1TLR (*35*)] using the program DS ViewerPro (Accelrys, Inc., San Diego). The value of X_1^r was set close to 0°, placing S_β in proximity to the C_5 H atom. The value of X_2^r was $\approx \pm 90°$, depending on the site and local steric interactions. Values of X_3^r and X_4^r were adjusted so that steric overlap between Rb and RNA was minimized. The carbon atoms of the nitroxide ring are in green, the nitrogen is in blue, and the oxygen is in red. The 4″-CH_3 substituent is in magenta.

the nitroxide at this site has the same correlation time as that estimated for the rotational diffusion of the entire molecule.

The models for 4-thio-U11Rb-TLR and 4-thio-U17Rb-TLR are not substantially different than that for 4-thio-U16Rb-TLR (not shown), and the origin of the interactions of the nitroxide ring with the RNA at these sites is not evident. However, the difference in mobility between Rb and Rc at U17 (Figure 5) does suggest that the 4″-CH_3 makes contact with the environment. Figure 7D is included to show the possible interaction of the 4″-CH_3 with a phosphate moiety in the backbone. The details and generality of correlation between the dynamics of the nitroxide label and local RNA structure will be the subject of future investigations.

Studies reported here are the first attempts on extracting information from base attached spin labels, and much more needs to be done to explore the limits of SDSL. For example, it is not clear whether one missing hydrogen bond will give rise to variations in RNA base motion that will alter the EPR spectrum, which is only sensitive to motions within 0.1−50 ns. It will also be interesting to investigate whether different EPR spectral characteristics might occur for base pairing variants, such as A/U and G/U. Further studies in other RNA systems, as well as the effects of mutations in the TLR system, will serve to address these issues.

ACKNOWLEDGMENT

We thank Drs. C. Altenbach and L. Columbus for valuable assistance in spectral simulation and interpretations, Dr. Ned van Eps for providing the spectrum of label R1c in T4 lysozyme, and members of the Feigon laboratory, particularly Drs. Robert Peterson, May Meroueh, Lukas Trantirek, Carla Theimer, David Finger, and Haihong Wu, for valuable assistance in NMR studies.

REFERENCES

1. Simons, R., and Grunberg-Manago, M. (1998) *RNA structure and function*, Cold Spring Harbor Laboratory Press, Cold Spring Harbor, NY.
2. Klein, D. J., Schmeing, T. M., Moore, P. B., and Steitz, T. A. (2001) *EMBO J. 20*, 4214−4221.
3. Akke, M., Fiala, R., Jiang, F., Patel, D., and Palmer, A. G. (1997) *RNA 3*, 702−709.
4. Hall, K. B., and Tang, C. (1998) *Biochemistry 37*, 9323−9332.
5. Dayie, K. T., Brodsky, A. S., and Williamson, J. R. (2002) *J. Mol. Biol. 317*, 263−278.
6. Hoogstraten, C. G., Wank, J. R., and Pardi, A. (2000) *Biochemistry 39*, 9951−9958.
7. Menger, M., Eckstein, F., and Porschke, D. (2000) *Biochemistry 39*, 4500−4507.
8. Bevilacqua, P., Kierzek, R., Johnson, K., and Turner, D. (1992) *Science 258*, 1355−1358.
9. Ha, T., Zhuang, X., Kim, H. D., Orr, J. W., Williamson, J. R., and Chu, S. (1999) *Proc. Natl. Acad. Sci. U.S.A. 96*, 9077−9082.
10. Zhuang, X., Bartley, L. E., Babcock, H. P., Russel, R., Ha, T., Herschlag, D., and Chu, S. (2000) *Science 288*, 2048−2051.
11. Zhuang, X., Kim, H., Pereira, M. J., Babcock, H. P., Walter, N. G., and Chu, S. (2002) *Science 296*, 1473−1476.
12. Kim, H. D., Nienhaus, G. U., Ha, T., Orr, J. W., Williamson, J. R., and Chu, S. (2002) *Proc. Natl. Acad. Sci. U.S.A. 99*, 4284−4289.
13. Zarrinkar, P. P., and Williamson, J. R. (1994) *Science 265*, 918−924.
14. Sclavi, B., Sullivan, M., Chance, M. R., Brenowitz, M., and Woodson, S. A. (1998) *Science 279*, 1940−1943.
15. Hubbell, W. L., and Altenbach, C. (1994) *Curr. Opin. Struct. Biol. 4*, 566−573.
16. Hubbell, W. L., Mchaourab, H. S., Altenbach, C., and Lietzow, M. A. (1996) *Structure 4*, 779−783.
17. Hubbell, W. L., Gross, A., Langen, R., and Leitzow, M. A. (1998) *Curr. Opin. Struct. Biol. 8*, 649−656.
18. Feix, J. B., and Klug, C. S. (1998) in *Biological Magnetic Resonance* (Berliner, L. J., Ed.) pp 251−281, Plenum Press, New York.
19. Hubbell, W. L., Cafiso, D. S., and Altenbach, C. (2000) *Nat. Struct. Biol. 7*, 735−739.
20. Fajer, P. G. (2000) in *Encyclopedia of analytical chemistry* (Meyers, R., Ed.) pp 5725−5761, John Wiley & Sons, Chichester.
21. Columbus, L., and Hubbell, W. L. (2002) *Trends Biochem. Sci. 27*, 288−295.
22. Columbus, L., Kalai, T., Jeko, J., Hideg, K., and Hubbell, W. L. (2001) *Biochemistry 40*, 3828−3846.
23. Isas, J. M., Langen, R., Haigler, H. T., and Hubbell, W. L. (2002) *Biochemistry 41*, 1464−1473.
24. Voss, J., Hubbell, W. L., and Kaback, H. R. (1998) *Biochemistry 37*, 211−216.
25. Altenbach, C., Oh, K. J., Trabanino, R. J., Hideg, K., and Hubbell, W. L. (2001) *Biochemistry 40*, 15471−15482.
26. Altenbach, C., Klein-Seetharaman, J., Cai, K., Khorana, H. G., and Hubbell, W. L. (2001) *Biochemistry 40*, 15493−15500.
27. Altenbach, C., Cai, K., Klein-Seetharaman, J., Khorana, H. G., and Hubbell, W. L. (2001) *Biochemistry 40*, 15483−15492.
28. Borbat, P. P., McHaourab, H. S., and Freed, J. H. (2002) *J. Am. Chem. Soc. 124*, 5304−5314.

29. Macosko, J. C., Pio, M. S., Tinoco, I., Jr., and Shin, Y.-K. (1999) *RNA 5*, 1158−1166.
30. Edwards, T. E., Okonogi, T. M., Robinson, B. H., and Sigurdsson, S. T. (2001) *J. Am. Chem. Soc. 123*, 1527−1528.
31. Qin, P. Z., Butcher, S. E., Feigon, J., and Hubbell, W. L. (2001) *Biochemistry 40*, 6929−6936.
32. Edwards, T. E., Okonogi, T. M., and Sigurdsson, S. T. (2002) *Chem. Biol. 9*, 699−706.
33. Ramos, A., and Varani, G. (1998) *J. Am. Chem. Soc. 120*, 10992−10993.
34. Costa, M., and Michel, F. (1995) *EMBO J. 14*, 1276−1285.
35. Butcher, S. E., Dieckmann, T., and Feigon, J. (1997) *EMBO J. 16*, 7490−7499.
36. Berliner, L. J., Grünwald, J., Hankovszky, H. O., and Hideg, K. (1982) *Anal. Biochem. 119*, 450−455.
37. Sar, C. P., Jeko, J., and Hideg, K. (1998) *Synthesis 30*, 1497−1500.
38. Hankovszky, H. O., Hideg, K., Lex, L., Kulcsar, G., and Halasz, H. A. (1982) *Can. J. Chem. 60*.
39. Breslauer, K. J. (1994) *Methods Mol. Biol. 26*, 347−372.
40. Langen, R., Cai, K., Altenbach, C., Khorana, H., and Hubbell, W. (1999) *Biochemistry 38*, 7918−7924.
41. Mchaourab, H. S., Lietzow, M. A., Hideg, K., and Hubbell, W. L. (1996) *Biochemistry 35*, 7692−7704.
42. Budil, D. E., Lee, S., Saxena, S., and Freed, J. H. (1996) *J. Magn. Reson., Ser. A 120*, 155−189.
43. Cantor, C. R., and Schimmel, P. R. (1980) in *Biophysical Chemistry*, pp 460−564, W. H. Freeman, San Francisco.
44. Coleman, R. S., and Kesicki, E. A. (1994) *J. Am. Chem. Soc. 116*, 11636−11642.
45. Kumar, R. K., and Davis, D. R. (1997) *Nucleic Acids Res. 25*, 1271−1280.
46. Butler, S. L., and Falke, J. J. (1996) *Biochemistry 35*, 10595−10600.
47. Barnes, J. P., Liang, Z., Mchaourab, H. S., Freed, J. H., and Hubbell, W. L. (1999) *Biophys. J. 76*, 3298−3306.
48. Hubbell, W. L., and McConnell, H. M. (1971) *J. Am. Chem. Soc. 93*, 314−326.
49. Langen, R., Oh, K. J., Cascio, D., and Hubbell, W. L. (2000) *Biochemistry 39*, 8396−8405.
50. Allain, F. H. T., and Varani, G. (1995) *J. Mol. Biol. 250*, 333−353.
51. Goldman, S. A., Bruno, G. V., and Freed, J. H. (1972) *J. Phys. Chem. 76*, 1858−1860.
52. Sutherland, I. O. (1971) in *Annual Reports on NMR Spectroscopy* (Mooney, E. S., Ed.) pp 71−225, Academic Press, London.
53. Fraser, R. R., Bousard, G., Saunders, J. K., Lambert, J. B., and Mixan, C. E. (1971) *J. Am. Chem. Soc. 93*, 3822.
54. Mchaourab, H. S., Kalai, T., Hideg, K., and Hubbell, W. L. (1999) *Biochemistry 38*, 2947−2955.
55. Snoussi, K., and Leroy, J. L. (2001) *Biochemistry 40*, 8898−8904.
56. Gueron, M., and Leroy, J. L. (1995) in *Methods in Enzymology* (James, T. L., Ed.) pp 383−413, Academic Press, San Diego.

BI027222P